remote sensing

MDPI

Article

Assessing the 2022 Flood Impacts in Queensland Combining Daytime and Nighttime Optical and Imaging Radar Data

Noam Levin [1,2,*] and Stuart Phinn [2]

[1] Department of Geography, Hebrew University of Jerusalem, Mount Scopus Campus, Jerusalem 91905, Israel
[2] Remote Sensing Research Center, School of Earth and Environmental Sciences, University of Queensland, St. Lucia, QLD 4072, Australia
* Correspondence: noamlevin@mail.huji.ac.il

Abstract: In the Australian summer season of 2022, exceptional rainfall events occurred in Southeast Queensland and parts of New South Wales, leading to extensive flooding of rural and urban areas. Here, we map the extent of flooding in the city of Brisbane and evaluate the change in electricity usage as a proxy for flood impact using VIIRS nighttime brightness imagery. Scanning a wide range of possible sensors, we used pre-flood and peak-flood PlanetScope imagery to map the inundated areas, using a new spectral index we developed, the Normalized Difference Inundation Index (NDII), which is based on changes in the NIR reflectance due to sediment-laden flood waters. We compared the Capella-Space X-band/HH imaging radar data captured at peak-flood date to the PlanetScope-derived mapping of the inundated areas. We found that in the Capella-Space image, significant flooded areas identified in PlanetScope imagery were omitted. These omission errors may be partly explained by the use of a single-date radar image, by the X-band, which is partly scattered by tree canopy, and by the SAR look angle under which flooded streets may be blocked from the view of the satellite. Using VIIRS nightly imagery, we were able to identify grid cells where electricity usage was impacted due to the floods. These changes in nighttime brightness matched both the inundated areas mapped via PlanetScope data as well as areas corresponding with decreased electricity loads reported by the regional electricity supplier. Altogether we demonstrate that using a variety of optical and radar sensors, as well as nighttime and daytime sensors, enable us to overcome data gaps and better understand the impact of flood events. We also emphasize the importance of high temporal revisit times (at least twice daily) to more accurately monitor flood events.

Keywords: floods; nighttime lights; electricity; VIIRS; PlanetScope

Citation: Levin, N.; Phinn, S. Assessing the 2022 Flood Impacts in Queensland Combining Daytime and Nighttime Optical and Imaging Radar Data. *Remote Sens.* **2022**, *14*, 5009. https://doi.org/10.3390/rs14195009

Academic Editor: Pinliang Dong

Received: 19 September 2022
Accepted: 5 October 2022
Published: 8 October 2022

1. Introduction

Remote sensing is now commonly used to map damages caused by extreme events [1,2], either natural disasters such as floods [3], fires [4], earthquakes [5], and volcanic eruptions [6], or human-caused disasters such as conflicts and wars [7,8]. Remote sensing mapping of flooding can be either directed at mapping inundated areas, most effectively using high spatial resolution optical imagery or using imaging radar data; [2,9] or for mapping building and property damage from flooding (most effectively using high spatial resolution optical imagery; [2]). While imaging radar data are probably most suited to map the inundated area given its capabilities to penetrate through cloud cover and forested areas [10], the temporal frequency and availability of analysis-ready imaging radar satellite data are lower than that available from optical satellites. The International Charter Space and Major Disasters was established in 1999 [11] to provide emergency response to countries in need from 17 charter members (space agencies and space system operators) as of 2022. Out of 765 activations globally, 405 activations were related to flood events, indicating the severity and frequency of floods and their societal impacts (https://cgt.disasterscharter.org/en, accessed on 27 July 2022). Nonetheless, Lindersson et al. [12] list just two globally available datasets of flood events: the

MODIS-NRT-FLOOD, which is available at a spatial resolution of 250 m [13], and the UNOSAT Flood Portal, which provides vector flood inundation maps for chosen flood events (299 altogether; http://floods.unosat.org/geoportal/catalog/search/search.page, accessed on 27 July 2022) using various satellites. On Google Earth Engine, the Global Flood Database v1 is available, containing maps of 913 large flood events between 2000 and 2018 as mapped by the Dartmouth Flood Observatory using MODIS imagery [14]. An additional floodwater fraction product based on the VIIRS sensor has recently become available [15,16] at a spatial resolution of 375 m, which can be downloaded from https://www.ssec.wisc.edu/flood-map-demo/flood-products/ (accessed on 11 September 2022), with historic datasets (from October 2019 onwards) to be downloaded from https://jpssflood.gmu.edu (accessed on 11 September 2022).

Given the relatively coarse spatial resolution of the MODIS and VIIRS flood products and their reliance on optical imagery, their mapping is impacted by cloud cover, and mapping of short-term and relatively small urban flood events is therefore not sufficient. More recently, the European Union has developed its Copernicus Emergency Management Service (CEMS), with one of its main focuses being the mapping of floods. Using the EU's Sentinel-1 SAR satellites, it can offer flood mapping products at a spatial resolution of 20 m (at full resolution; [17,18]). Out of 564 rapid CEMS activations, 199 activations were for flood events (https://emergency.copernicus.eu/mapping, accessed on 28 July 2022). Martinis et al. [19] have recently demonstrated that fusing optical and imaging radar data can enhance the mapping of seasonal surface reference water masks, which is important for improving flood mapping products. However, given that frequently, flooded areas (aside from seasonal floodplains) stay inundated for short periods ranging from hours to days, the temporal revisit time is critical for mapping inundated areas. In Australia, the Water Observation from Space (WOfS) product (based on the Landsat image archive) offers annual mapping of the percent frequency of water cover [20]. While this is an excellent product, it is not well suited to map areas that were inundated for a short period of time, given the relatively low revisit time of Landsat. Wang et al. [21] suggested the use of volunteered passenger photos taken from aircraft as an additional source for mapping flooded areas; however, this is not an operational option.

Given the limitations of currently available flood products, our aim was to demonstrate the combined use of high-resolution spatial daytime optical imagery and nighttime lights imagery to assess the impact of floods within urban areas for recent flood events which took place in Southeast Queensland (SEQ) and northern New South Wales (NSW), Australia, in February and March 2022.

2. Materials and Methods

2.1. Study Area

Brisbane is the capital city of Queensland and is Australia's third largest metropolitan area, with about 1.2 million residing within the Brisbane City Council area and about 2.6 million people living within Greater Brisbane (estimates for 2021). Brisbane is located in a sub-tropical climate area, with an average annual rainfall of 1,148 mm. Located on the flood plain of the Brisbane River, many suburbs of Brisbane are found in flood-prone areas, with the largest recorded historical floods taking place in 1841, 1893, 1974, and 2011 [22–24].

Previous studies on mapping flood events in Brisbane and Southeast Queensland used a variety of approaches: a combination of volunteered geographic photography of maximum flood levels and Lidar-generated DEM to generate a digital flood surface over central Brisbane for the flood event of January 2011 [25]; a two-dimensional hydrodynamic model using bathymetric data for the flood events of January 2011 and January 2013 (achieving an accuracy of 66.9%; [26]); mapping flood events using a fully convolutional neural networks classification model from single date Landsat images [27]; estimating disaster severity through an analysis of reports on social media [28]; mapping flooded areas under vegetation using single SAR image acquisition [29]; flood hazard susceptibility modeling using deep learning neural networks [30]. One of the challenges in mapping

the extent of inundated areas is that flood levels recede relatively fast, and it is unlikely that satellite images will be acquired at the time of maximum flood height. Therefore, a combination of pre-flood, co-flood, and post-flood data and imagery is recommended for mapping inundated areas [31].

The flood events studied here are those that took place in SEQ and northern NSW at the end of February and beginning of March 2022 [32]. These floods were predicted given the consecutive two years of La Niña [33] and resulted in extreme multi-day rain and flooding in SEQ and eastern NSW between 22 February and 9 March 2022, with more than 50 sites in those areas recording more than 1000 mm of rainfall in the week ending 1 March 2022 [34]. The Brisbane City Gauge recorded 792.9 mm over the six days between 23 and 28 February 2022, being 78% of the annual average of that site [34]. However, the magnitude of the extent and impacts of the floods, primarily in northern NSW, was not predicted.

Within this research, flood gauge analyses were run for all Queensland (QLD) and NSW, nighttime lights analyses were run within SEQ and northern NSW, and the delineation of inundated areas from satellite images was performed for parts of the area of Greater Brisbane (Figure 1).

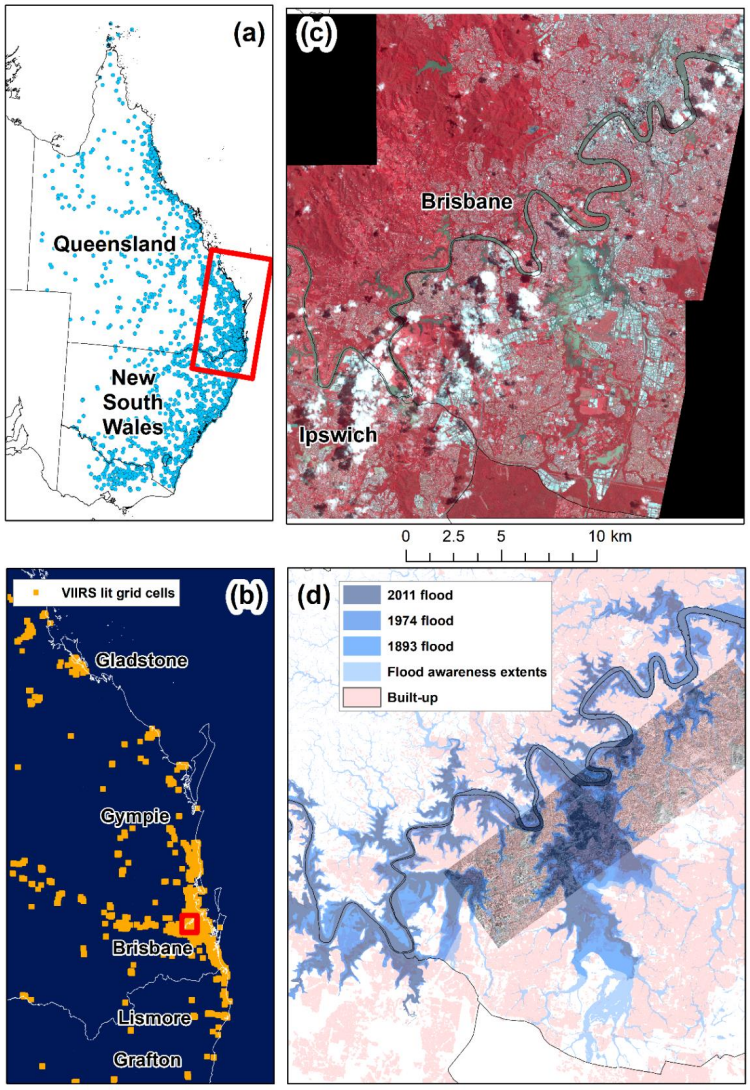

Figure 1. Study area: (**a**) Bureau of Meteorology river gauge stations in Queensland and New South Wales; (**b**) VIIRS lit grid cells which were analyzed; (**c**) PlanetScope imagery from peak flood day in Brisbane, 28/2/2022; (**d**) past extent floods in Brisbane and built-up areas (from the global urban footprint; Esch et al., 2017) with the Capella SAR image acquired on 28 February 2022 in the background.

2.2. Data Sets

2.2.1. Flood Gauge Data

The flood height data were downloaded from the Australian Bureau of Meteorology from the following URL: ftp://ftp.bom.gov.au/anon2/home/ncc/srds/FloodingInEasternAustraliaFebMar2022/ (accessed on 13 March 2022). This dataset included river gauge measurements between 13 February 2022 and 4 March 2022 (19 days) for 2635 stations, 1428 in QLD and 1208 in NSW. Data completeness and the frequency of river height measurements varied between and within stations. For example, in the St. Lucia Alert station (BoM #540683), there were 2249 height measurements within this time frame, of which 98.6% were valid data. Overall, the median number of measurements per station was 1238 (with 90% of the stations having more than 167 measurements), and the median percentage of valid measurements (not flagged as void) was 99% (with 90% of the stations having more than 84% of valid measurements). For each station, we calculated the average and standard deviation of the pre-flood heights (between the dates 4 and 23 February 2022), the maximum and 99th percentile of the flood levels, the difference between the maximum height and mean pre-flood levels, and the date when maximum level height was attained.

2.2.2. Nighttime Lights Data

Remote sensing of night lights provides an excellent approach for monitoring human activity from space [35] and has also been used to monitor the impact of natural and anthropogenic disasters on the supply of electricity [8,36]. To examine the impact of flood events on artificial nighttime lights, we used the nightly VIIRS Black Marble product of VNP46A1 [37]. This product provides nightly sensor with top-of-atmosphere radiance (in units of nW cm^{-2} sr^{-1}) and a spatial resolution of 15 arc s (~450 m at the equator; https://ladsweb.modaps.eosdis.nasa.gov/missions-and-measurements/products/VNP46A1/; accessed on 11 August 2022). We downloaded all of the nightly products of granule h33v11 between calendar days 39 and 86 (8 February 2022 and 27 March 2022, 48 days). This granule covers all of Queensland (east of longitude 150°E) and north-eastern NSW (north of latitude 30°S). Within QLD, it covers cities from Rockhampton in the north to Brisbane, Ipswich, and the Gold Coast in the south, and within NSW, it covers towns from Grafton in the south to Lismore and Tweed Heads in the north. For our analysis, we only included cloud-free pixels from each of the nights (based on the VNP46A1 cloud mask status). We extracted all of the lit grid cells (grid cells where the brightness value in 2016 was greater than 5 nW cm^{-2} sr^{-1}; n = 11,628) within this granule and divided the time frame into three main periods: (1) pre-flood (8–23 February 2022); (2) peak and post-flood I (1–14 March 2022); and (3) post-flood II (15–27 March 2022). We ran *t*-tests to examine whether brightness levels differed between periods 1 and 2 (areas impacted by floods may record a decrease in nighttime brightness levels) and between periods 2 and 3 (areas recovering from floods may record an increase in nighttime brightness levels). Given that we analyzed more than 10,000 grid cells, we only considered the grid cells to be statistically significant cells where the *p*-value of the *t*-test was less than 0.01. We also calculated the difference and ratio between the brightness levels of periods 1 and 2 and between periods 2 and 3.

2.2.3. PlanetScope Satellite Imagery

Given that there were no cloud-free images of Sentinel 2, Landsat 8, or Landsat 9 over Brisbane and Ipswich, which corresponded with the dates of peak flooding, we used the PlanetScope images. To represent the peak flood, we used the PlanetScope data acquired on 28 February 2022, and we compared it with the pre-flood PlanetScope images acquired on 9 February 2022 (which covered Brisbane) and 17 February 2022 (which covered the city of Ipswich, south-west of Brisbane). Whereas the mapping of inundated areas from optical satellites is often based on a single data image using normalized difference indices (e.g., [38]), we preferred an approach that was based on change detection [31]. We considered using the Normalized Difference Water Index (NDWI; [39]), which is based

on the green and NIR bands; however, we found that the NDWI misclassified many built areas as inundated areas, as already noted by Xu [40]. We could not apply versions of the NDWI, which are using a middle IR (MIR) band [40,41] because the PlanetScope imagery does not have an MIR band. Therefore, we took a different approach. Following a flood, the NIR reflectance decreases dramatically. We, therefore, developed the following spectral index to identify inundated areas (the Normalized Difference Inundation Index), based on spectral differences in the NIR band, before the flood and during peak flooding:

$$NDII = \frac{NIR_{pre-flood} - NIR_{peak-flood}}{NIR_{pre-flood} + NIR_{peak-flood}} \quad (1)$$

We used a threshold of NDII > 0.1 to identify inundated areas based on the histogram of the NDII values. Because some areas were affected by clouds and cloud shadows, either in the pre-flood or the post-flood images, we manually edited and removed false-positive areas, which were misidentified as inundated due to clouds and cloud shadows. An additional approach we used to identify and remove false positives was based on the LiDAR DEM (areas that were too high to be flooded) and based on the mapping of Brisbane City Council of "areas at risk of flooding" (pixels with NDII values greater than 0.1 outside the areas at risk of flooding were in the vast majority identified as false positives). In our mapping of inundated areas, we focused on inundated patches with an area larger than 0.1 ha.

2.2.4. Supporting Datasets

LiDAR

We used Australia's national Digital Elevation Model (DEM derived from LiDAR 5 m Grid (Geoscience Australia, 2015) to evaluate flood height levels and to validate our mapping of inundated areas.

SAR and Optical Imagery for Validation

Very few imaging radar data were available for the time of peak flood over Brisbane. We examined potential sources from Sentinel 1a and 1b, Capella-Space, Iceye and the NovaSAR satellite. Sentinel 1b was not functional at this time; hence we were limited to captures by 1a over the study area. We could not locate suitable Sentinel 1a or Iceye data and used Capella-Space and NovaSAR data. For north-eastern NSW, the NovaSAR image from 5 March 2022 was able to map many flooded areas, and the NovaSAR image from 6 March 2022 over Brisbane was well after the flood peak.

Sentinel 1 did not have any overpass over Brisbane during the time of the floods (although it did pass over northern NSW to cover the flooded areas there). The Copernicus EMS Rapid Mapping activity provided a very localized map of the inundated areas for central Brisbane based on a rather cloudy image acquired by GeoEye on 28 February 2022 (https://emergency.copernicus.eu/mapping/list-of-components/EMSR567/ALL/EMSR567_AOI03, accessed on 16 August 2022).

We also had access to Capella X-band imaging radar data [42]. The Capella image was acquired on 28 February 2022, covering an area to the south of the Brisbane River at a spatial resolution of 0.8 m. The image was slant and ground-range corrected, orthorectified, and corrected to normalized radar backscatter coefficient. We resampled the Capella image to 3.2 m to fit the spatial resolution of the PlanetScope image. To remove speckle noise, we ran an adaptive box filter [43] on the image three times, using the following parameters: a threshold standard deviation of 0.75 within a 7×7 moving window, replacing invalid pixels with local averages. Following filtering, we applied a threshold (<230) to map inundated areas, to serve as a comparison for our mapping of inundated areas in Brisbane based on the PlanetScope image.

Inundated Areas from Past Floods and Hydrography

Historical flood extents (for the flood events of 1893, 1974, and 2011) and areas at risk of flooding (from one or more sources: river, creek, overland flow, and storm tide inside the Brisbane City Council local government area) were downloaded from https://www.spatial-data.brisbane.qld.gov.au/search?collection=Dataset (accessed on 12 August 2022). These datasets were downloaded to compare the 2022 flood extent in Brisbane with historical flood extents. To show the hydrography of the rivers, we used the dataset of Hydrosheds [44].

Electricity Load

We used the Energex (the company supplying electricity to Southeast Queensland) zone substation load data reports for the year 2021–2022 (providing raw load data in MW measured in half-hourly intervals), available from https://www.energex.com.au/about-us/company-information/our-network/zone-substation-load-data-reports (accessed on 28 August 2022). A point layer of these substations was available from https://qldspatial.information.qld.gov.au/catalogue/custom/search.page (accessed on 28 August 2022). We divided the time frame into two main periods, focusing only on weekdays (given that over the weekend power loads are lower): (1) weekdays preceding the flood (21–25 February 2022); (2) weekdays during the main flooding period (28 February–4 March 2022). We ran *t*-tests to examine whether brightness levels differed between periods 1 and 2 (areas impacted by floods may record a decrease in electricity loads). Given that we analyzed about 240 stations, we only considered zones statistically significant where the *p*-value of the t-test was less than 0.01.

3. Results

The date(s) at which maximum river heights were reached ranged from 24 February 2022 (for SE QLD) to 4 March 2022 (Figures 2 and 3). However, in most stations along the Brisbane River, the dates of maximum river height were either 27 February or 28 (Figures 2 and 3). Within the Brisbane River, the maximum river height increased upriver, from about 3.9 m at the Brisbane Post Office (city center) to 8 m at Corinda, 13 m at Goodna, and more than 16m, upstream at Ipswich (Figure 3).

The most significant differences in the PlanetScope reflectance data between the pre-flood and the peak-flood images were found in the NIR band, with flooding leading to a significant reduction in reflectance in the NIR for both vegetated areas (e.g., grass) and roads (Figure 4). This was the main reason for our choice to construct the Normalized Difference Inundation Index (NDII) based on pre-flood and peak-flood NIR bands (Figure 5). Note that for the Brisbane River, floodwater raised the reflectance in the NIR, given the greater sediment load, leading the river to appear to be brighter (Figures 4 and 6a,b). The NDII values for flooded vegetation and roads were well above 0.1 (Figure 5), whereas areas usually covered by water (such as the Brisbane River) had negative NDII values (Figure 5), providing a clear separation between inundated areas and permanent water bodies (Figure 6c). However, cloud cover in either the pre-flood image or the peak-flood image led to the identification of false positives in our mapping of inundated areas, especially where there was a cloud in the pre-flood image or where there were cloud shadows in the peak flood image (Figures 5 and 6c). We, therefore, masked out areas of clouds and cloud shadows to derive our map of inundated areas (Figure 6d). The 2022 flood in Brisbane was a bit lower than the 2011 flood; on 13 January 2011, the flood peaked in the Brisbane City Alert station at the height of 4.46 m (http://www.bom.gov.au/qld/flood/fld_history/brisbane_history.shtml; accessed on 25 August 2022), whereas on 28 February 2022 the river reached a maximum height of 3.85 m at the same place (Figure 3). While many areas were flooded in Brisbane (see photos from the suburb of St. Lucia, Figure 7), fewer areas were inundated in Brisbane in 2022 in comparison with 2011 (Figure 6d).

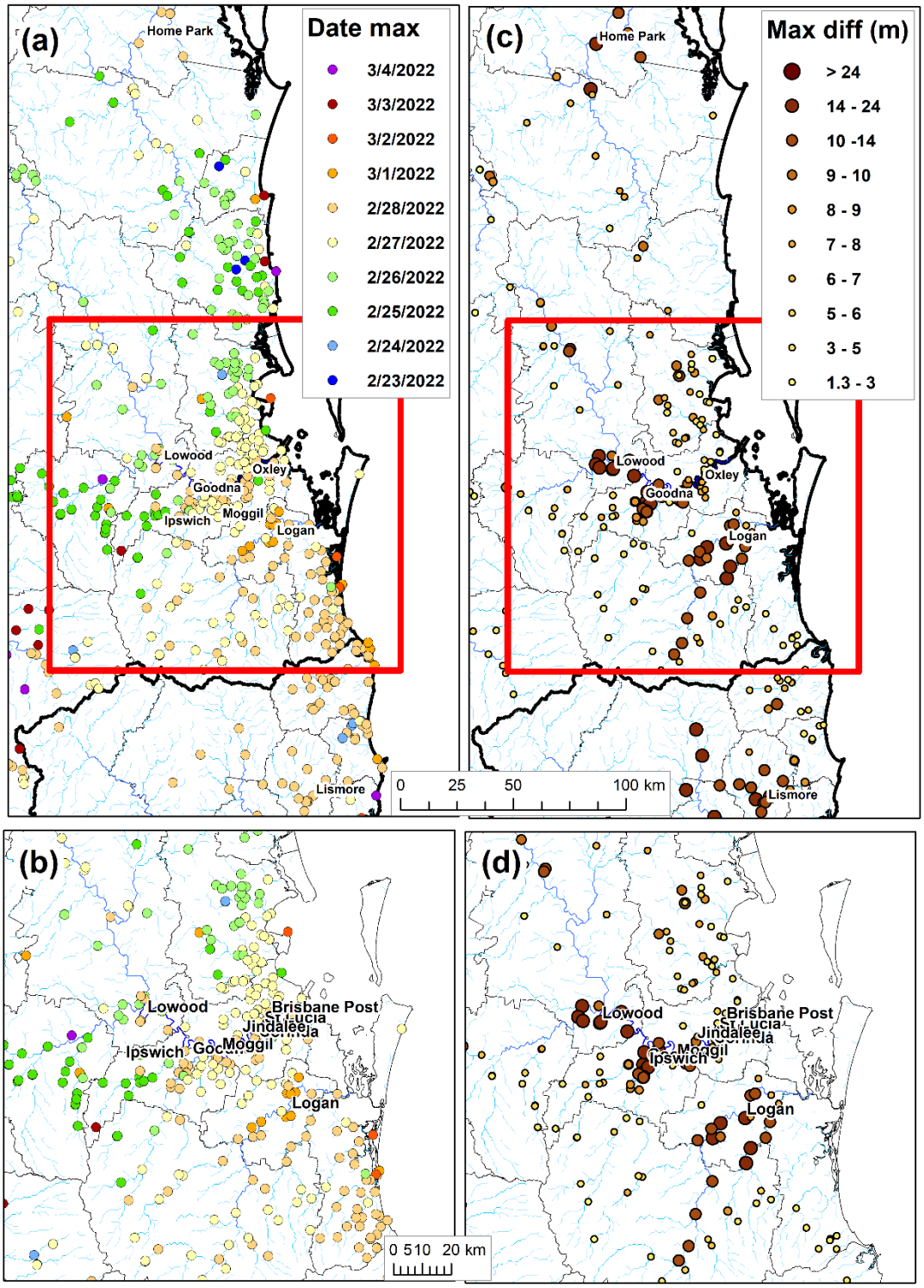

Figure 2. Australian Bureau of Meteorology (BoM) river gauge stations: Date of maximum river height (**a**,**b**), and the difference (m) between maximum river height and the pre-flood height (**c**,**d**). The temporal changes in river height are shown in Figure 3 for the labeled stations. The station of Home Park is located on the Mary River, north of Gympie. The rivers were derived from the global Hydrosheds dataset [44]. The extent of the maps in (**b**,**d**) is shown by a red line in (**a**,**c**).

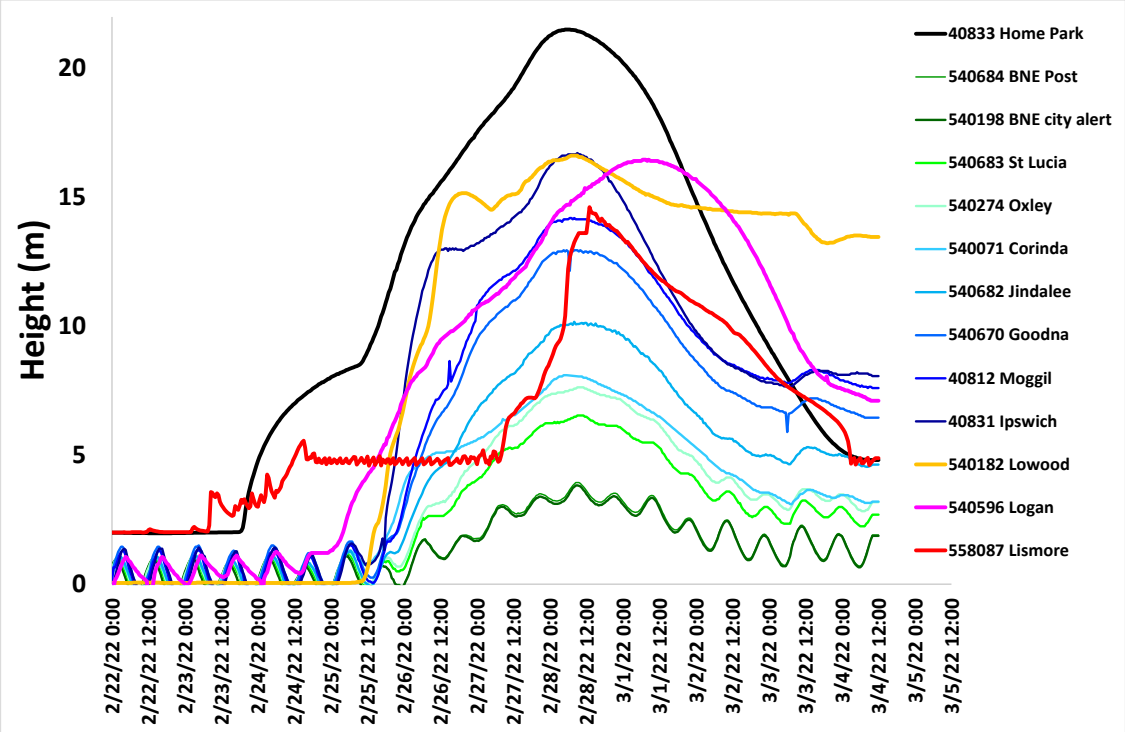

Figure 3. Temporal changes in river height between 22 February 2022 and 4 March 2022 for selected river height stations (their locations are shown in Figure 2). The numbers preceding a station's (shortened) name represent its serial number as given by the Australian Bureau of Meteorology (BoM).

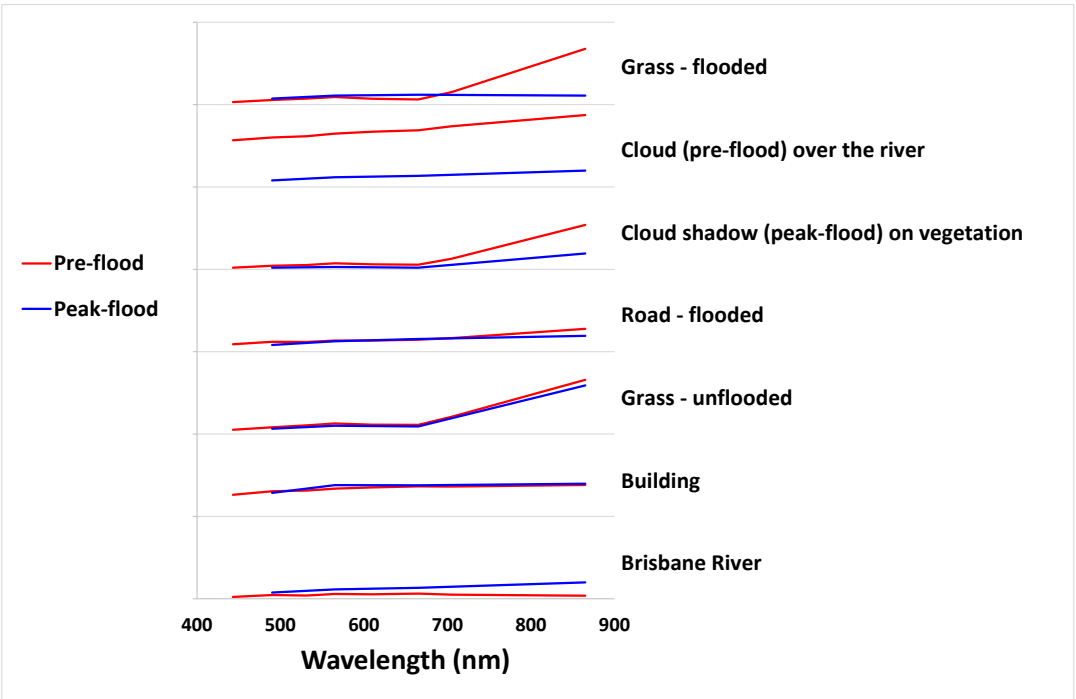

Figure 4. Representative spectra over flooded and unflooded sites, comparing data from the pre-flood 8-band PlanetScope image (9 February 2022) and the peak-flood 4-band PlanetScope image (28 February 2022).

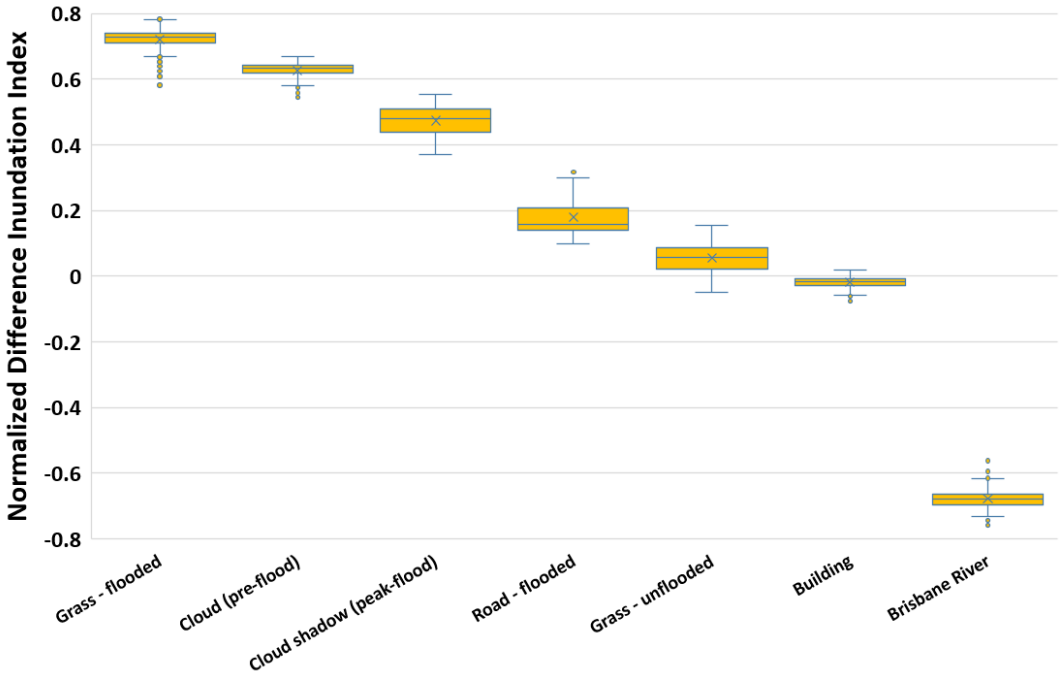

Figure 5. Box plots of the Normalized Difference Inundation Index (NDII) values for the regions of interest shown in Figure 4. We used a threshold of 0.1 to distinguish between flooded and unflooded areas. Note that pre-flood cloud or post-flood cloud shadows lead to false positives.

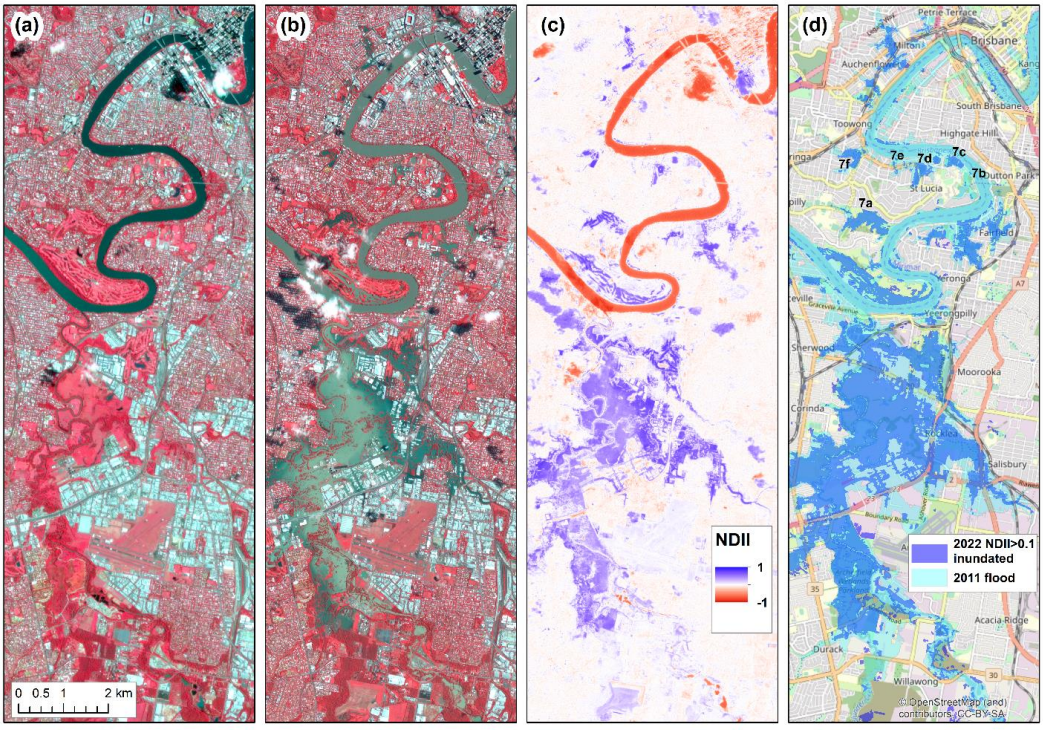

Figure 6. (**a**) Pre-flood PlanetScope image, 9 February 2022, showing the area from Brisbane's CBD in the north, through the St. Lucia campus of the University of Queensland, to the flood plain of Oxley Creek in the south; (**b**) Peak-flood PlanetScope image, 28 February 2022; (**c**) NDII map; (**d**) Comparison between the 2011 flood, and the areas inundated in 2022 (after removal of false-positives). The approximate locations of photos taken on 28 February 2022 are shown here, the photos are presented in Figure 7.

Figure 7. Photos of the flood taken on 28 February 2022 in the suburb of St. Lucia. The locations of the photos are shown in Figure 6. (**a**) The St. Lucia Golf Course; (**b**) The CityCat ferry station of the University of Queensland on the Brisbane River; (**c**) University of Queensland fields (ovals) no. 6 and 7; (**d**) William Dart Park (note the inundated soccer goal); (**e**) St. Lucia Market on Sir Fred Schonell Drive; (**f**) Heroes Avenue between Jack Cook Memorial Park and Perrin Park.

The Capella SAR image acquired on 28 February 2022 covered a smaller area than the PlanetScope image; however it did cover significant areas of the Oxley Creek flood plain to allow comparison between the two mapping approaches of inundated areas. Using the Capella image, we identified less inundated areas; however, many inundated areas were clearly omitted in the Capella mapping (Figure 8).

The flooding had a clear impact on electricity loads as reported by Energex for SEQ (Figure 9a,b) and on nighttime brightness as measured by VIIRS (Figure 9c,d). Out of 240 substation zones of Energex, in 133 zones (55%), there was a statistically significant decrease in electricity loads on the weekdays between the pre-flood week (21–25 February 2022) and flood week (28 February–4 March 2022). Out of 11,236 lit grid cells within the VIIRS tile which we analyzed, in 953 grid cells (8.5%), there was a statistically significant decrease in nighttime brightness between the pre-flood period (8–23 February 2022) and the peak and post-flood period (1–14 March 2022). Amongst the 37 local government areas (LGAs) included within the VIIRS tile, several LGAs were more severely affected than others by the floods. In Lismore (NSW), 60% of all lit grid cells experienced a statistically significant decrease in nighttime brightness, and in several other LGAs (Byron, Clarence Valley, Gympie, Richmond Valley, and Tweed), between 20 and 28% of all of the lit grid cells were impacted. In absolute numbers, the largest number of lit VIIRS grid cells that were impacted by the floods was in Brisbane, where in 176 (5%) of the grid cells, there was a significant decrease. Zooming in on Brisbane, it is possible to see a good match between

the inundated areas and the VIIRS lit grid cells where there was a statistically significant decrease in nighttime brightness, especially in the Oxley Creek floodplain (Figure 9d). The location of Energex substation zones in which electricity loads were impacted also seemed to fit the inundation map; however, these zones are much coarser (Figure 9b). To demonstrate the impact of the floods over the temporal scale, we focus on two areas: the Oxley Creek flood plain (Figure 10) and the town of Gympie (Figure 11). In both cases, a clear decrease in electricity loads can be observed, which started already on February 24th in Gympie, and on 26 February in the Oxley Creek area. VIIRS nighttime brightness data were not available (due to cloud cover) during the nights when most of the rain fell; however, once the clouds have dispersed, the darkening of both areas is clearly observed, as well as the gradual recovery of nighttime brightness in the following two weeks after the flood (Figures 10 and 11). In 44% of the grid cells where a statistically significant decrease in nighttime brightness was observed between the pre-flood period and the peak and post-flood period I, a statistically significant increase in nighttime brightness was observed between peak and post-flood period I and post-flood period II.

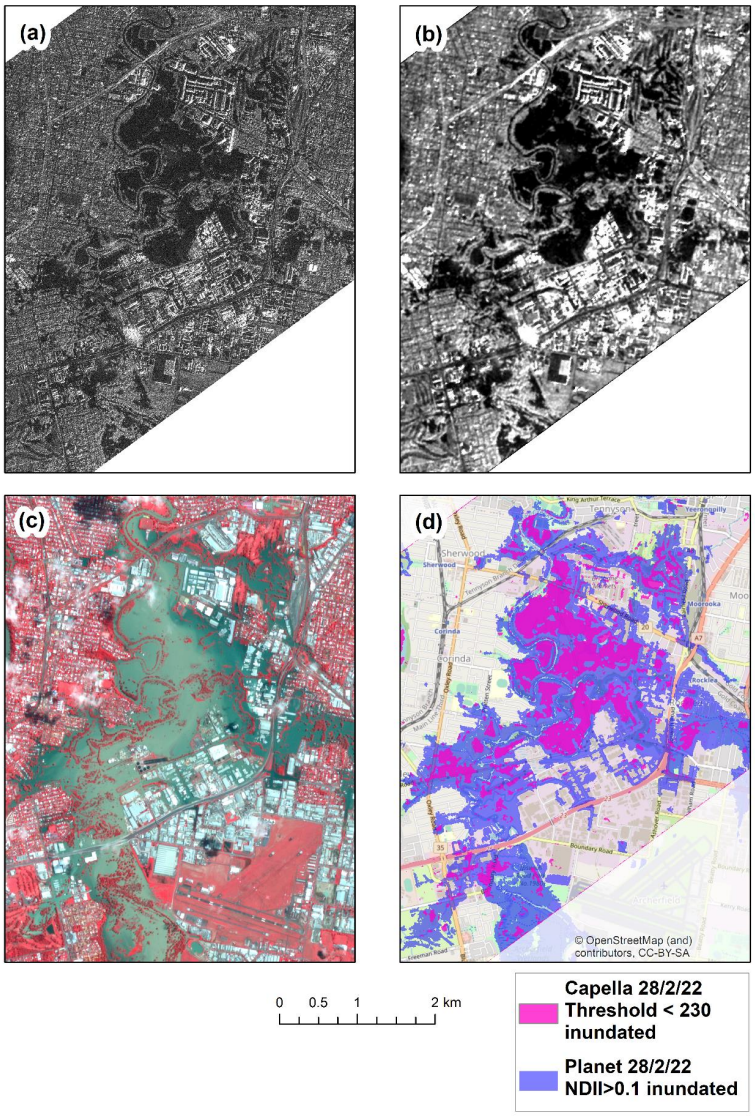

Figure 8. Comparison of inundated areas mapping from PlanetScope (based on change detection) and Capella (single image): (**a**) Capella image (28 February 2022) resampled to 3.2 m; (**b**) Capella image after running an adaptive box filter three times; (**c**) False color composite PlanetScope image, 28 February 2022; (**d**) Inundated areas derived from the PlanetScope and Capella images.

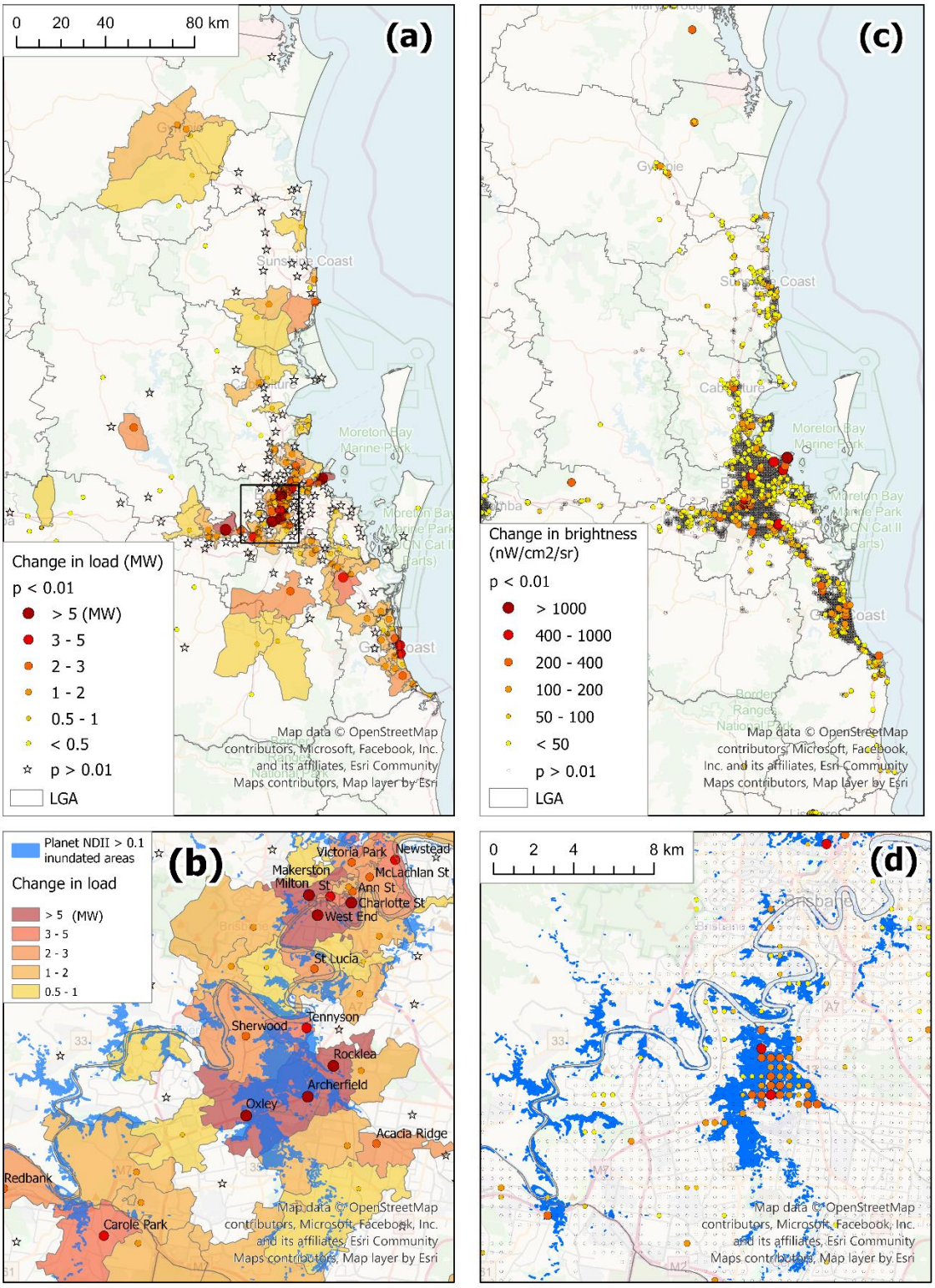

Figure 9. The impact of floods on electricity loads (based on Energex data for substation zones; (**a**,**b**)) and on nighttime brightness (from VIIRS nightly data; (**c**,**d**)), comparing pre-flood period values and during flood period values (periods defined in the Methods). All changes shown indicate a decrease in energy use due to the impacts of the floods. In both datasets, only changes where the statistical significance of the *t*-test was below 0.01 are shown. The inset maps zooming on Brisbane (**b**,**d**) also show the inundated areas based on the PlanetScope image.

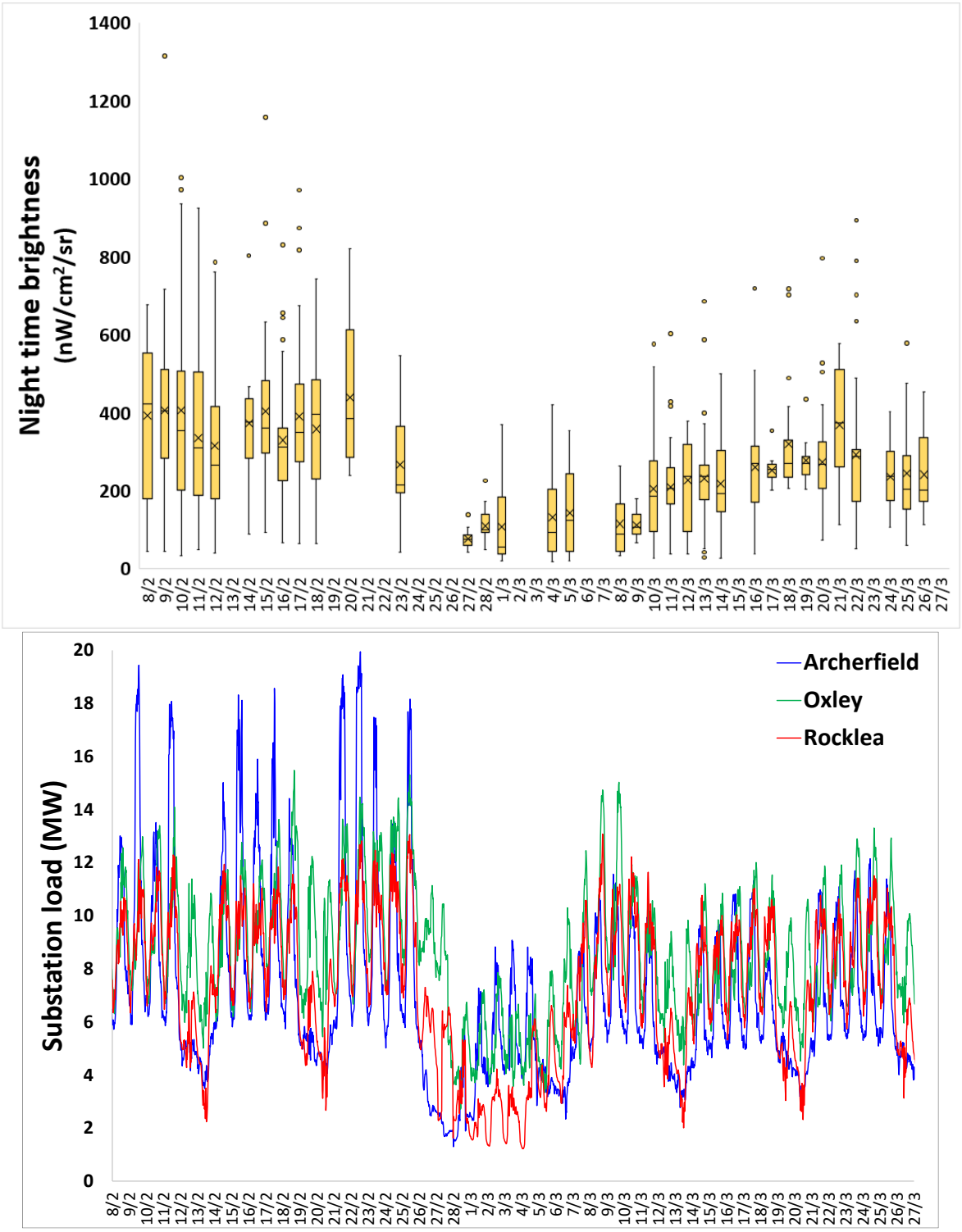

Figure 10. Top: Box plot of nighttime brightness for 40 VIIRS grid cells in the Oxley Creek floodplain where there was a statistically significant difference in nighttime brightness between period 1 and period 2. Bottom: Substation electricity loads (half-hourly data from Energex) for three substation zones corresponding with the Oxley Creek floodplain. The boxplot only includes cloud-free data.

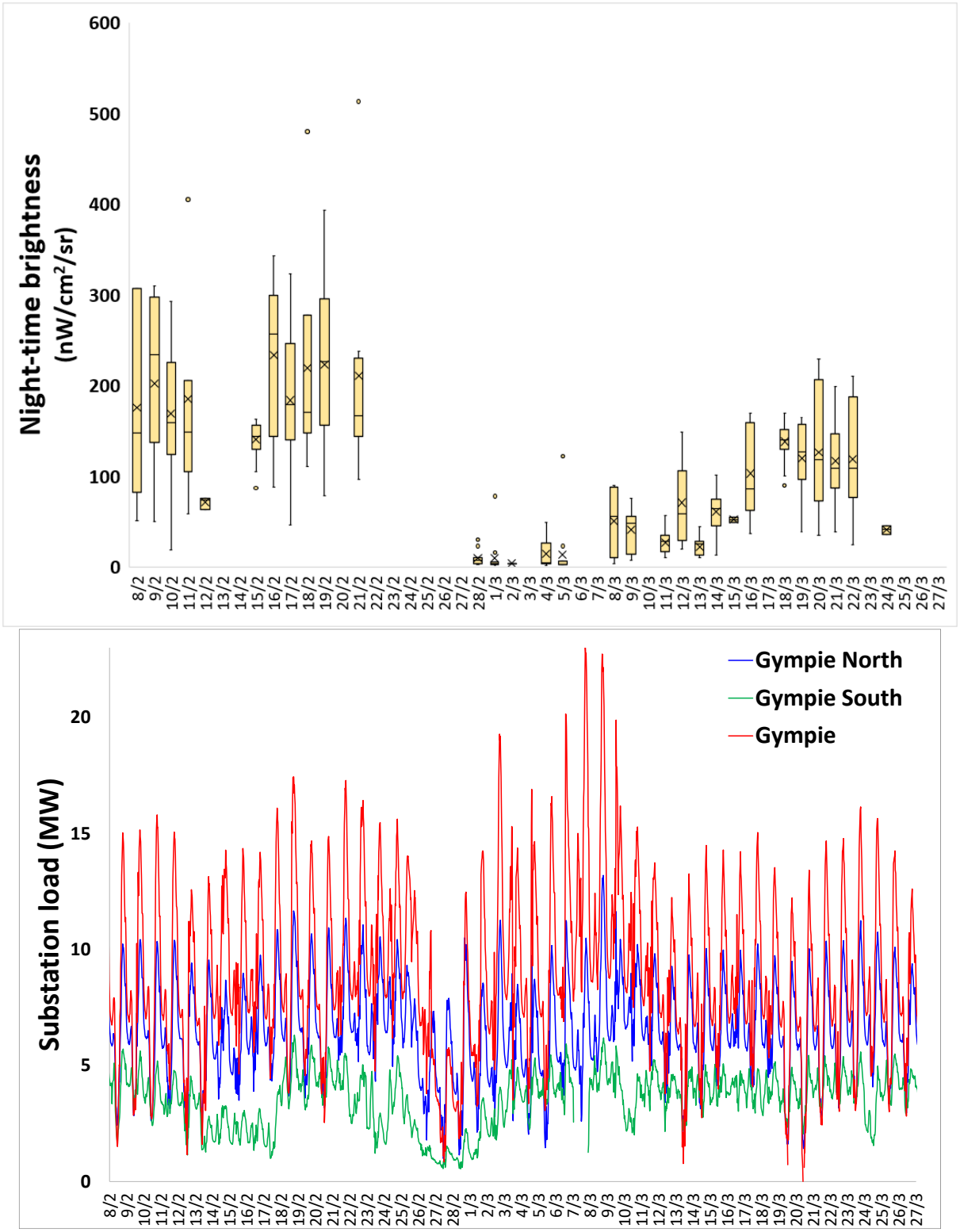

Figure 11. Top: Box plot of nighttime brightness for 16 VIIRS grid cells in Gympie where there was a statistically significant difference in nighttime brightness between period 1 and period 2. Bottom: Substation electricity loads (half-hourly data from Energex) for three substation zones covering Gympie. The boxplot only includes cloud-free data.

4. Discussion

Mapping water bodies is a complex operation in coastal, inland–tidal, and inland water bodies if it is performed correctly, and a number of well-established and tested approaches have been developed both at global and local scales (e.g., [45]) for mapping the shoreline to differentiate between land and water (e.g., [46,47]). Generally, water bodies absorb almost all of the solar energy in the near-infrared and absorb all of it in the short-wave infrared; hence they are quite separable from land features. However, mapping flood events within urban areas (in contrast with flood events in rural areas, which often cover huge areas; [48]) in subtropical climates introduces several challenges in comparison with mapping year-round deep-water bodies. (1) River water in flood events is sediment-laden, and hence, they are brighter than usual ([49]). (2) Flood events within urban areas are usually brief, and waters often recede within a few days; hence a high temporal revisit of the sensor is crucial for successful mapping of the inundated areas [50]. (3) During flood events, cloud cover is common, especially in sub-tropical regions, and hence SAR is often a better choice than optical sensors for mapping flood events, given its cloud penetration capabilities [9].

In our case study of mapping inundated areas in SEQ, very few imaging radar data were available at the time of the peak flood event, and hence we used PlanetScope images, which offer a daily revisit time, given the size of this constellation of satellites [51]. However, a daily revisit time is often not enough, and while parts of the image were affected by cloud cover, we were fortunate that most of the urban areas of Brisbane were cloud-free. To map the inundated areas, we developed a new spectral index, the normalized difference inundation index (NDII), which is based on a normalized difference between the pre-flood image and the peak-flood image. Spectral indices, which are based on change detection, are commonly used in mapping burn severity, e.g., by calculating the difference in the values of a spectral index between a pre-fire and a post-fire image [52]. Whereas for mapping burnt areas, a post-fire image can be used (given that in most cases, it takes time for vegetation to recover following a fire event), to map areas that were inundated for a short time of just a few days, a post-flood image often will not suffice, because vegetation will not be much affected (compare with the impact of more severe flooding on crops: [53]). Hence, our index required an image representing the flood when it was near its peak. Inundated areas are now mapped using complex decision trees (e.g., [15]) or using deep learning and machine learning techniques [54]; however, one of the advantages of the index we developed is the simplicity of its calculation. In addition, because of the spectral changes in NIR reflectance following a flood event, both on land and for river water, the NDII clearly distinguishes between flooded areas (positive NDII values) and permanent water bodies through which sediment-laden flood waters are flowing (negative NDII values). Comparing our mapping of inundated areas from the PlanetScope image with mapping of the inundated areas from a Capella imaging radar data set, we found that the PlanetScope image enabled us to map much larger areas and that many of the inundated areas delineated using PlanetScope, were omitted in the imaging radar mapping (Figure 8). While the imaging radar data had a higher spatial resolution, we did not have at our disposal a comparable pre-flood imaging radar data set, which might have aided in this mapping. In addition, given the slant angle in which imaging radar data are acquired, within urban areas, the view of the ground is likely obstructed by buildings and trees (Capella's look angle range is between 25° and 40°; [55]), which may also hamper the mapping of inundated areas. Furthermore, the X-band of Capella likely interacts with tree canopies, whereas longer wavelength SAR bands (such as Sentinel 1′s C band) may be better at penetrating through trees [56]. While Capella promises to be the first operational constellation of commercial SAR satellites, and one of its development motivations is to enable real-time mapping of flood events [56], it has not reached its full promised constellation of 36 satellites, which will enable a one-hour revisit time. Optical sensors, which offer a closer to nadir geometry, have some advantages for mapping inundation within urban areas, especially where buildings are higher and streets narrower. Using images acquired during the flood (whether optical or imaging radar)

resembles the use of active fire hotspots for monitoring wildfires from space; however, in both cases, the key requirement is that there will be an overpass of a satellite at the time of the event.

Given that the flood waters receded in less than a week for most areas in Brisbane, there were not many visible impacts on vegetated areas in the parks and riparian areas (other than trees that stood close to the river and were under direct impact). While mapping inundated areas usually requires that the overpass of a sensor will coincide with the time of the flood, some impacts of the flood can be mapped from space days later. Here, we refer to flood impacts on infrastructure and especially to the impacts on electricity usage. Changes in observed nighttime lights have been suggested as a means to estimate the impacts of natural disasters, including floods, and their effectiveness depends on the availability of cloud-free images and on whether the area under study is a lit area [57]. Analyzing the time series of the cloud-free grid cells from the VIIRS VNP46A1 nightly product [37], we were able to identify grid cells that were darkened following the floods, even without taking into account variability in the view angles of the VIIRS [58]. Although the cloud-free data were often not available for some of the days (with or without rainfall), there were enough data to identify the grid cells that were impacted and thus to map impacted areas based on the temporal signature of their nighttime brightness. The impacted areas were also verified using official electricity loads available from the regional electricity provider, Energex. While electricity load data provide official and highly reliable information at a high temporal frequency, such data are not available across all countries, and the spatial units in which it was available were quite coarse. Using the VIIRS nighttime brightness enables us to disaggregate such spatial units [59,60], Energex substation zones in our case, and to identify the exact locations where the supply and use of electricity were impacted. Using VIIRS nighttime brightness, the magnitude of the impact of a natural disaster, as well as the recovery from it, can be quantified [36].

Whereas wildfires can spread widely wherever fuel is available for burning, given an ignition event and appropriate meteorological conditions [61], areas at risk of inundation are spatially constrained to riparian and floodplain areas. Another key difference between wildfires and flood events is related to their temporal properties. Once a forest has burnt, it will often take the vegetation at least several years before there will be enough fuel for another fire. However, the same area may be flooded again and again, and in fact, within a single rain season, previous flooding only enhances the likelihood of a subsequent flood event if the soil is still saturated [24]. With climate change, the likelihood of flood events will change, although predictions are difficult to be made, given the complexity of this phenomenon and the uncertainty in the key drivers of extreme rainfall [62]. However, one thing is certain: remote sensing will remain key to monitoring floods and understanding their extent, duration, and impacts.

5. Conclusions

Floods represent a recurring and significant hazard globally and in Australia. Monitoring inundation in urban areas is associated with specific challenges, given the more limited duration and area of flood events, requiring high temporal revisit times of sensors (at least twice daily), either optical or imaging radar. Using a spectral index that is based on changes in the NIR reflectance, the NDII, we were able to map inundated areas in Brisbane using pre-flood and peak-flood PlanetScope images. While emerging imaging radar constellations may provide an operational mapping of floods in the future, we show that already the impacts of floods on the electricity supply for the population can be mapped using VIIRS nighttime brightness images. We believe that a multi-sensor approach is highly useful when tackling complex natural disaster events, where different sensors assist in validating each other and in tracking different aspects of rolling events.

Author Contributions: Conceptualization, N.L.; methodology, N.L. and S.P.; validation, N.L.; formal analysis, N.L.; investigation, N.L.; resources, N.L. and S.P.; data curation, N.L.; writing—original draft preparation, N.L.; writing—review and editing, N.L. and S.P.; visualization, N.L. All authors have read and agreed to the published version of the manuscript.

Funding: This research received no external funding.

Data Availability Statement: Almost all data used in this study (other than the Capella SAR image) are publicly and freely available, and we provide the links to the datasets in the methods. Once our paper is published, we will make our own derived datasets (e.g., of inundated areas) available online.

Acknowledgments: We would like to thank Patrick Ward and Cathy Toby, Climate Data Services, Bureau of Meteorology (BoM), for assistance in accessing river height data, and Chris Woodman at Energy Queensland, for assistance in accessing the spatial dataset of the substation zones of Energex. We also thank Peleg Kark-Levin for pre-processing the BoM river gauge data. Satellite image data were provided for research use by Planet Inc and Capella Space Inc.

Conflicts of Interest: The authors declare no conflict of interest.

References

1. Tralli, D.M.; Blom, R.G.; Zlotnicki, V.; Donnellan, A.; Evans, D.L. Satellite Remote Sensing of Earthquake, Volcano, Flood, Landslide and Coastal Inundation Hazards. *ISPRS J. Photogramm. Remote Sens.* **2005**, *59*, 185–198. [CrossRef]
2. Joyce, K.E.; Belliss, S.E.; Samsonov, S.V.; McNeill, S.J.; Glassey, P.J. A Review of the Status of Satellite Remote Sensing and Image Processing Techniques for Mapping Natural Hazards and Disasters. *Prog. Phys. Geogr. Earth Environ.* **2009**, *33*, 183–207. [CrossRef]
3. Klemas, V. Remote Sensing of Floods and Flood-Prone Areas: An Overview. *J. Coast. Res.* **2014**, *31*, 1005–1013. [CrossRef]
4. Lentile, L.B.; Holden, Z.A.; Smith, A.M.S.; Falkowski, M.J.; Hudak, A.T.; Morgan, P.; Lewis, S.A.; Gessler, P.E.; Benson, N.C. Remote Sensing Techniques to Assess Active Fire Characteristics and Post-Fire Effects. *Int. J. Wildland Fire* **2006**, *15*, 319–345. [CrossRef]
5. Dong, L.; Shan, J. A Comprehensive Review of Earthquake-Induced Building Damage Detection with Remote Sensing Techniques. *ISPRS J. Photogramm. Remote Sens.* **2013**, *84*, 85–99. [CrossRef]
6. Blackett, M. An Overview of Infrared Remote Sensing of Volcanic Activity. *J. Imaging* **2017**, *3*, 13. [CrossRef]
7. Witmer, F.D.W. Remote Sensing of Violent Conflict: Eyes from Above. *Int. J. Remote Sens.* **2015**, *36*, 2326–2352. [CrossRef]
8. Levin, N.; Ali, S.; Crandall, D. Utilizing Remote Sensing and Big Data to Quantify Conflict Intensity: The Arab Spring as a Case Study. *Appl. Geogr.* **2018**, *94*, 1–17. [CrossRef]
9. Parker, A.L.; Castellazzi, P.; Fuhrmann, T.; Garthwaite, M.C.; Featherstone, W.E. Applications of Satellite Radar Imagery for Hazard Monitoring: Insights from Australia. *Remote Sens.* **2021**, *13*, 1422. [CrossRef]
10. Smith, L.C. Satellite Remote Sensing of River Inundation Area, Stage, and Discharge: A Review. *Hydrol. Process.* **1997**, *11*, 1427–1439. [CrossRef]
11. Stryker, T.; Jones, B. Disaster Response and the International Charter Program. *Photogramm. Eng. Remote Sens.* **2009**, *2009*, 1342–1344.
12. Lindersson, S.; Brandimarte, L.; Mård, J.; Di Baldassarre, G. A Review of Freely Accessible Global Datasets for the Study of Floods, Droughts and Their Interactions with Human Societies. *WIREs Water* **2020**, *7*, e14242020. [CrossRef]
13. Policelli, F.; Slayback, D.; Brakenridge, B.; Nigro, J.; Hubbard, A.; Zaitchik, B.; Carroll, M.; Jung, H. The NASA Global Flood Mapping System. In *Remote Sensing of Hydrological Extremes*; Lakshmi, V., Ed.; Springer Remote Sensing/Photogrammetry; Springer International Publishing: Cham, Switzerland, 2017; pp. 47–63; ISBN 978-3-319-43744-6.
14. Tellman, B.; Sullivan, J.A.; Kuhn, C.; Kettner, A.J.; Doyle, C.S.; Brakenridge, G.R.; Erickson, T.A.; Slayback, D.A. Satellite Imaging Reveals Increased Proportion of Population Exposed to Floods. *Nature* **2021**, *596*, 80–86. [CrossRef]
15. Li, S.; Sun, D.; Goldberg, M.D.; Sjoberg, B.; Santek, D.; Hoffman, J.P.; DeWeese, M.; Restrepo, P.; Lindsey, S.; Holloway, E. Automatic near Real-Time Flood Detection Using Suomi-NPP/VIIRS Data. *Remote Sens. Environ.* **2018**, *204*, 672–689. [CrossRef]
16. Li, S.; Sun, D.; Goldberg, M.D.; Kalluri, S.; Sjoberg, B.; Lindsey, D.; Hoffman, J.P.; DeWeese, M.; Connelly, B.; Mckee, P.; et al. A Downscaling Model for Derivation of 3-D Flood Products from VIIRS Imagery and SRTM/DEM. *ISPRS J. Photogramm. Remote Sens.* **2022**, *192*, 279–298. [CrossRef]
17. Matgen, P.; Martinis, S.; Wagner, W.; Freeman, V.; Zeil, P.; McCormick, N. Feasibility Assessment of an Automated, Global, Satellite-Based Flood-Monitoring Product for the Copernicus Emergency Management Service. Available online: https://elib.dlr.de/130247/ (accessed on 16 September 2022).
18. Salamon, P.; Mctlormick, N.; Reimer, C.; Clarke, T.; Bauer-Marschallinger, B.; Wagner, W.; Martinis, S.; Chow, C.; Böhnke, C.; Matgen, P.; et al. The New, Systematic Global Flood Monitoring Product of the Copernicus Emergency Management Service. In Proceedings of the 2021 IEEE International Geoscience and Remote Sensing Symposium IGARSS, Brussels, Belgium, 11–16 July 2021; pp. 1053–1056.
19. Martinis, S.; Groth, S.; Wieland, M.; Knopp, L.; Rättich, M. Towards a Global Seasonal and Permanent Reference Water Product from Sentinel-1/2 Data for Improved Flood Mapping. *Remote Sens. Environ.* **2022**, *278*, 113077. [CrossRef]

20. Mueller, N.; Lewis, A.; Roberts, D.; Ring, S.; Melrose, R.; Sixsmith, J.; Lymburner, L.; McIntyre, A.; Tan, P.; Curnow, S.; et al. Water Observations from Space: Mapping Surface Water from 25years of Landsat Imagery across Australia. *Remote Sens. Environ.* **2016**, *174*, 341–352. [CrossRef]
21. Wang, C.; Ke, J.; Xiu, W.; Ye, K.; Li, Q. Emergency Response Using Volunteered Passenger Aircraft Remote Sensing Data: A Case Study on Flood Damage Mapping. *Sensors* **2019**, *19*, 4163. [CrossRef]
22. Van den Honert, R.C.; McAneney, J. The 2011 Brisbane Floods: Causes, Impacts and Implications. *Water* **2011**, *3*, 1149–1173. [CrossRef]
23. Cook, M. Vacating the Floodplain: Urban Property, Engineering, and Floods in Brisbane (1974–2011). *Conserv. Soc.* **2017**, *15*, 344–354. [CrossRef]
24. Cook, M. *A River with a City Problem: A History of Brisbane Floods*; Univ. of Queensland Press: Brisbane, Australia, 2019.
25. McDougall, K.; Temple-Watts, P. The Use of LiDAR and Volunteered Geographic Information to Map Flood Extents and Inundation. *ISPRS Ann. Photogramm. Remote Sens. Spat. Inf. Sci.* **2012**, *1–4*, 251–256. [CrossRef]
26. Liu, X.; Lim, S. Flood Inundation Modelling for Mid-Lower Brisbane Estuary. *River Res. Appl.* **2017**, *33*, 415–426. [CrossRef]
27. Sarker, C.; Mejias, L.; Maire, F.; Woodley, A. Flood Mapping with Convolutional Neural Networks Using Spatio-Contextual Pixel Information. *Remote Sens.* **2019**, *11*, 2331. [CrossRef]
28. Kankanamge, N.; Yigitcanlar, T.; Goonetilleke, A.; Kamruzzaman, M. Determining Disaster Severity through Social Media Analysis: Testing the Methodology with South East Queensland Flood Tweets. *Int. J. Disaster Risk Reduct.* **2020**, *42*, 101360. [CrossRef]
29. Grimaldi, S.; Xu, J.; Li, Y.; Pauwels, V.R.N.; Walker, J.P. Flood Mapping under Vegetation Using Single SAR Acquisitions. *Remote Sens. Environ.* **2020**, *237*, 111582. [CrossRef]
30. Kalantar, B.; Ueda, N.; Saeidi, V.; Janizadeh, S.; Shabani, F.; Ahmadi, K.; Shabani, F. Deep Neural Network Utilizing Remote Sensing Datasets for Flood Hazard Susceptibility Mapping in Brisbane, Australia. *Remote Sens.* **2021**, *13*, 2638. [CrossRef]
31. Giordan, D.; Notti, D.; Villa, A.; Zucca, F.; Calò, F.; Pepe, A.; Dutto, F.; Pari, P.; Baldo, M.; Allasia, P. Low Cost, Multiscale and Multi-Sensor Application for Flooded Area Mapping. *Nat. Hazards Earth Syst. Sci.* **2018**, *18*, 1493–1516. [CrossRef]
32. Vardoulakis, S.; Matthews, V.; Bailie, R.S.; Hu, W.; Salvador-Carulla, L.; Barratt, A.L.; Chu, C. Building Resilience to Australian Flood Disasters in the Face of Climate Change. *Med. J. Aust.* **2022**, *217*, 342–345. [CrossRef]
33. McCormack, L. Aussie Hydrologist Predicts Floods . . . Again. *News Weekly*, 23 March 2022. Available online: https://ncc.org.au/newsweekly/energy-science-enviro/aussie-hydrologist-predicts-flooding-again/ (accessed on 19 September 2022).
34. Bureau of Meteorology. *Special Climate Statement 76—Extreme Rainfall and Flooding in South-Eastern Queensland and Eastern New South Wales*; Bureau of Meteorology: Melbourne, VIC, Australia, 2022.
35. Levin, N.; Kyba, C.C.M.; Zhang, Q.; Sánchez de Miguel, A.; Román, M.O.; Li, X.; Portnov, B.A.; Molthan, A.L.; Jechow, A.; Miller, S.D.; et al. Remote Sensing of Night Lights: A Review and an Outlook for the Future. *Remote Sens. Environ.* **2020**, *237*, 111443. [CrossRef]
36. Román, M.O.; Stokes, E.C.; Shrestha, R.; Wang, Z.; Schultz, L.; Carlo, E.A.S.; Sun, Q.; Bell, J.; Molthan, A.; Kalb, V.; et al. Satellite-Based Assessment of Electricity Restoration Efforts in Puerto Rico after Hurricane Maria. *PLoS ONE* **2019**, *14*, e0218883. [CrossRef]
37. Román, M.O.; Wang, Z.; Sun, Q.; Kalb, V.; Miller, S.D.; Molthan, A.; Schultz, L.; Bell, J.; Stokes, E.C.; Pandey, B.; et al. NASA's Black Marble Nighttime Lights Product Suite. *Remote Sens. Environ.* **2018**, *210*, 113–143. [CrossRef]
38. Wan, K.M.; Billa, L. Post-Flood Land Use Damage Estimation Using Improved Normalized Difference Flood Index (NDFI3) on Landsat 8 Datasets: December 2014 Floods, Kelantan, Malaysia. *Arab. J. Geosci.* **2018**, *11*, 434. [CrossRef]
39. McFeeters, S.K. The Use of the Normalized Difference Water Index (NDWI) in the Delineation of Open Water Features. *Int. J. Remote Sens.* **1996**, *17*, 1425–1432. [CrossRef]
40. Xu, H. Modification of Normalised Difference Water Index (NDWI) to Enhance Open Water Features in Remotely Sensed Imagery. *Int. J. Remote Sens.* **2006**, *27*, 3025–3033. [CrossRef]
41. Gao, B. NDWI—A Normalized Difference Water Index for Remote Sensing of Vegetation Liquid Water from Space. *Remote Sens. Environ.* **1996**, *58*, 257–266. [CrossRef]
42. Stringham, C.; Farquharson, G.; Castelletti, D.; Quist, E.; Riggi, L.; Eddy, D.; Soenen, S. The Capella X-Band SAR Constellation for Rapid Imaging. In Proceedings of the IGARSS 2019–2019 IEEE International Geoscience and Remote Sensing Symposium, Yokohama, Japan, 28 July–2 August 2019; pp. 9248–9251.
43. Eliason, E.M.; McEwen, A.S. Adaptive Box Filters for Removal of Random Noise from Digital Images. *Photogramm. Eng. Remote Sens.* **1990**, *56*, 453–458.
44. Lehner, B.; Grill, G. Global River Hydrography and Network Routing: Baseline Data and New Approaches to Study the World's Large River Systems. *Hydrol. Process.* **2013**, *27*, 2171–2186. [CrossRef]
45. Pekel, J.-F.; Cottam, A.; Gorelick, N.; Belward, A.S. High-Resolution Mapping of Global Surface Water and Its Long-Term Changes. *Nature* **2016**, *540*, 418–422. [CrossRef]
46. Murray, N.J.; Phinn, S.R.; DeWitt, M.; Ferrari, R.; Johnston, R.; Lyons, M.B.; Clinton, N.; Thau, D.; Fuller, R.A. The Global Distribution and Trajectory of Tidal Flats. *Nature* **2019**, *565*, 222–225. [CrossRef]
47. Bishop-Taylor, R.; Nanson, R.; Sagar, S.; Lymburner, L. Mapping Australia's Dynamic Coastline at Mean Sea Level Using Three Decades of Landsat Imagery. *Remote Sens. Environ.* **2021**, *267*, 112734. [CrossRef]

48. Mirza, M.M.Q. Climate Change, Flooding in South Asia and Implications. *Reg. Environ. Chang.* **2011**, *11*, 95–107. [CrossRef]
49. Brodie, J.; Schroeder, T.; Rohde, K.; Faithful, J.; Masters, B.; Dekker, A.; Brando, V.; Maughan, M. Dispersal of Suspended Sediments and Nutrients in the Great Barrier Reef Lagoon during River-Discharge Events: Conclusions from Satellite Remote Sensing and Concurrent Flood-Plume Sampling. *Mar. Freshw. Res.* **2010**, *61*, 651–664. [CrossRef]
50. Panteras, G.; Cervone, G. Enhancing the Temporal Resolution of Satellite-Based Flood Extent Generation Using Crowdsourced Data for Disaster Monitoring. *Int. J. Remote Sens.* **2018**, *39*, 1459–1474. [CrossRef]
51. Strauss, M. Planet Earth to Get a Daily Selfie. *Science* **2017**, *355*, 782–783. [CrossRef]
52. Key, C.H.; Benson, N.C. *Landscape Assessment (LA): Sampling and Assessment Methods FIREMON: Fire Effects Monitoring and Inventory System*; U.S. Department of Agriculture, Forest Service, Rocky Mountain Research Station: Fort Collins, CO, USA, 2006; pp. 1–55.
53. Rahman, M.; Di, L.; Yu, E.; Lin, L.; Yu, Z. Remote Sensing Based Rapid Assessment of Flood Crop Damage Using Novel Disaster Vegetation Damage Index (DVDI). *Int. J. Disaster Risk Sci.* **2021**, *12*, 90–110. [CrossRef]
54. Hashemi-Beni, L.; Gebrehiwot, A.A. Flood Extent Mapping: An Integrated Method Using Deep Learning and Region Growing Using UAV Optical Data. *IEEE J. Sel. Top. Appl. Earth Obs. Remote Sens.* **2021**, *14*, 2127–2135. [CrossRef]
55. Castelletti, D.; Farquharson, G.; Stringham, C.; Duersch, M.; Eddy, D. Capella Space First Operational SAR Satellite. In Proceedings of the 2021 IEEE International Geoscience and Remote Sensing Symposium IGARSS, Brussels, Belgium, 11–16 July 2021; pp. 1483–1486.
56. Yague-Martinez, N.; Leach, N.R.; Dasgupta, A.; Tellman, E.; Brown, J.S. Towards Frequent Flood Mapping with the Capella Sar System. The 2021 Eastern Australia Floods Case. In Proceedings of the 2021 IEEE International Geoscience and Remote Sensing Symposium IGARSS, Brussels, Belgium, 11–16 July 2021; pp. 6174–6177.
57. Zhao, X.; Yu, B.; Liu, Y.; Yao, S.; Lian, T.; Chen, L.; Yang, C.; Chen, Z.; Wu, J. NPP-VIIRS DNB Daily Data in Natural Disaster Assessment: Evidence from Selected Case Studies. *Remote Sens.* **2018**, *10*, 1526. [CrossRef]
58. Kyba, C.C.M.; Aubé, M.; Bará, S.; Bertolo, A.; Bouroussis, C.A.; Cavazzani, S.; Espey, B.R.; Falchi, F.; Gyuk, G.; Jechow, A.; et al. Multiple Angle Observations Would Benefit Visible Band Remote Sensing Using Night Lights. *J. Geophys. Res. Atmos.* **2022**, *127*, e2021JD036382. [CrossRef]
59. Stevens, F.R.; Gaughan, A.E.; Linard, C.; Tatem, A.J. Disaggregating Census Data for Population Mapping Using Random Forests with Remotely-Sensed and Ancillary Data. *PLoS ONE* **2015**, *10*, e01070422015. [CrossRef]
60. Liu, X.; Ou, J.; Wang, S.; Li, X.; Yan, Y.; Jiao, L.; Liu, Y. Estimating Spatiotemporal Variations of City-Level Energy-Related CO2 Emissions: An Improved Disaggregating Model Based on Vegetation Adjusted Nighttime Light Data. *J. Clean. Prod.* **2018**, *177*, 101–114. [CrossRef]
61. Bradstock, R.A. A Biogeographic Model of Fire Regimes in Australia: Current and Future Implications. *Glob. Ecol. Biogeogr.* **2010**, *19*, 145–158. [CrossRef]
62. Johnson, F.; White, C.J.; van Dijk, A.; Ekstrom, M.; Evans, J.P.; Jakob, D.; Kiem, A.S.; Leonard, M.; Rouillard, A.; Westra, S. Natural Hazards in Australia: Floods. *Clim. Chang.* **2016**, *139*, 21–35. [CrossRef]